THE JOURNAL OF PHYSICAL CHEMISTRY B

Article

pubs.acs.org/JPCB

The Most Effective Gold Nanorod Size for Plasmonic Photothermal Therapy: Theory and *In Vitro* Experiments

Megan A. Mackey, Moustafa R. K. Ali,† Lauren A. Austin,† Rachel D. Near,† and Mostafa A. El-Sayed*

Laser Dynamics Laboratory, School of Chemistry and Biochemistry, Georgia Institute of Technology, Atlanta, Georgia 30332-0400, United States

Supporting Information

ABSTRACT: The development of new and improved photothermal contrast agents for the successful treatment of cancer (or other diseases) via plasmonic photothermal therapy (PPTT) is a crucial part of the application of nanotechnology in medicine. Gold nanorods (AuNRs) have been found to be the most effective photothermal contrast agents, both *in vitro* and *in vivo*. Therefore, determining the optimum AuNR size needed for applications in PPTT is of great interest. In the present work, we utilized theoretical calculations as well as experimental techniques *in vitro* to determine this optimum AuNR size by comparing plasmonic properties and the efficacy as photothermal contrast agents of three different sizes of AuNRs. Our theoretical calculations showed that the contribution of absorbance to the total extinction, the electric field, and the distance at which this field extends away from the nanoparticle surface all govern the effectiveness of the amount of heat these particles generate upon NIR laser irradiation. Comparing between three different AuNRs (38 × 11, 28 × 8, and 17 × 5 nm), we determined that the 28 × 8 nm AuNR is the most effective in plasmonic photothermal heat generation. These results encouraged us to carry out *in vitro* experiments to compare the PPTT efficacy of the different sized AuNRs. The 28 × 8 nm AuNR was found to be the most effective photothermal contrast agent for PPTT of human oral squamous cell carcinoma. This size AuNR has the best compromise between the total amount of light absorbed and the fraction of which is converted to heat. In addition, the distance at which the electric field extends from the particle surface is most ideal for this size AuNR, as it is sufficient to allow for coupling between the fields of adjacent particles in solution (i.e., particle aggregates), resulting in effective heating in solution.

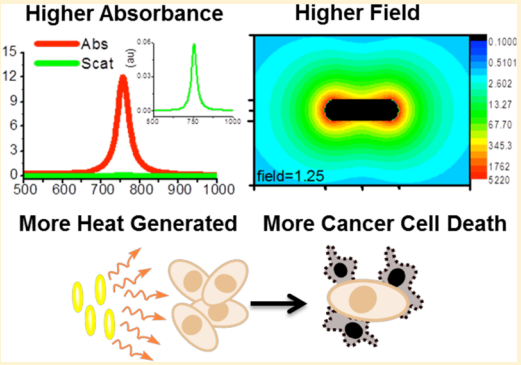

INTRODUCTION

Plasmonic photothermal therapy (PPTT) for the treatment of cancer has received a great deal of attention in recent years, especially with the advent of new photothermal contrast agents.[1] In the past decade, specifically, there has been much progress in the development of plasmonic nanoparticles for photothermal therapy applications due to their unique optical properties, namely, their localized surface plasmon resonance (LSPR),[2,3] as well as their inherently low toxicities.[4−6] The unique plasmonic properties of nanoparticles can be exploited in photothermal therapy by coherently photoexciting their conduction electrons to induce surface plasmon oscillations. Upon surface plasmon formation, nonradiative relaxation occurs through electron−phonon and phonon−phonon coupling, efficiently generating localized heat that can be transferred to the surrounding environment.[3,7,8] This conversion of photon energy to thermal energy is useful in biomedical applications, such as plasmonic photothermal therapy of cancer.[9−13]

In PPTT, thermal energy generated can induce temperature increases of more than 20 °C (i.e., hyperthermia), which can thereby induce tumor tissue ablation.[10−12,14−19] This was first demonstrated *in vitro*, by Lin and co-workers in 2003, using antibody-conjugated spherical gold nanoparticle-labeled lymphocytes and a nanosecond pulsed visible laser.[20] A few years later, El-Sayed and co-workers also used visible light and antibody-conjugated spherical gold nanoparticles for the selective photothermal ablation of epithelial carcinoma cells *in vitro*.[9] Although visible light is successful in destroying cells labeled with spherical gold nanoparticles, the need for radiation to penetrate deep into tissues, with minimal attenuation by water and hemoglobin, is desired for the practical application of PPTT. Near-infrared (NIR) external radiation is capable of achieving this, such that it can penetrate up to 10 cm in soft tissues (termed the NIR tissue transmission window, 650−900 nm).[21] By changing the shape and composition of the nanoparticle, the surface plasmon absorption can be shifted into the NIR transmission window.[22−27] With this in mind, gold nanoparticles (AuNPs) that absorb in the NIR tissue transmission window were developed by Halas and co-workers (silica−gold core−shell nanoparticles),[11,18] El-Sayed and co-workers (rod-shaped AuNPs),[12,28] as well as Xia and co-

Received: September 17, 2013
Revised: January 9, 2014
Published: January 16, 2014

   dx.doi.org/10.1021/jp409298f | J. Phys. Chem. B 2014, 118, 1319−1326

workers (gold nanocages).[29] When comparing the different nanoparticle structures in terms of their application in PPTT, the most important plasmonic properties to consider are the absorption cross section and the absorption efficiency, as these govern the thermal transduction per particle.[30,31] Of all the plasmonic AuNPs developed, the rod-shaped AuNPs, or gold nanorods (AuNRs), exhibit the most ideal NIR absorption cross section[32] and demonstrate extremely efficient NIR photothermal heat conversion.[17] The most common size of AuNR utilized for use in successful PPTT now is around 40 nm in length and 10 nm in diameter, with a longitudinal plasmon resonance around 800 nm. Investigating various AuNR sizes, specifically those that have smaller dimensions, and their efficacy as photothermal contrast agents has important implications in the clinical applications of AuNRs in PPTT. Also, as previously shown theoretically by Jain et al., plasmonic absorption becomes dominant as the nanoparticle size is decreased.[30,31] More specifically, the extinction of the AuNRs increases with the size of the AuNRs, while the contribution of scattering also increases, essentially decreasing the absorbance:scattering ratio as the AuNR size increases. This ultimately suggests that, as the particle size decreases, the absorbance:scattering ratio increases, allowing for greater photothermal heat conversion and therefore potentially enhancing PPTT efficacy with decreased particle size. Another plasmonic property associated with photothermal heat conversion is the electric field at the surface of the AuNR. It has previously been shown that excitation at the plasmon wavelength creates very strong electromagnetic fields,[33,34] and the field strength trends with absorbance, not scattering or extinction.[35] Since the field strength is derived from absorbance, not scattering, greater absorbance with smaller AuNRs would indicate a stronger field, which in turn would result in greater photothermal heat conversion and, again, enhanced PPTT efficacy.

In this work, we present both theoretical and experimental results, comparing the AuNRs commonly used for PPTT (about 38 × 11 nm) and two new, smaller AuNRs[36] (about 28 × 8 nm and 17 × 5 nm), in order to determine which would be the most effective photothermal contrast agent. The discrete dipole approximation (DDA), a theoretical technique for modeling the spectral properties of varying nanoparticle shapes, was utilized for the theoretical portion of this work. DDA has the advantage of being able to model particles of arbitrary shape.[30,34,37−40] In this method, the particle is represented by a three-dimensional finite lattice of point dipoles that is excited by an external field. The response of the point dipoles to the external field and to one another is solved self-consistently using Maxwell's equations. The DDSCAT 6.1 code offered publicly by Draine and Flatau[41] allows for the calculation of the absorbance and scattering spectra separately, enabling the assessment of the contributions from each to the extinction spectra, which is ideal for comparing the overall absorbance and absorbance:scattering ratios of the three different sizes of AuNRs. Furthermore, with modifications to the code by Goodman[42] and Schatz,[43] it is possible to calculate the electric field enhancement contours and the individual dipole orientations at a specific wavelength, allowing for the theoretical estimation of the potential heat generated by the different-sized AuNRs upon exposure to NIR radiation. Theoretical results show that the electromagnetic field around the particle and the absorbance:scattering ratio increase as the AuNR size decreases. Experimental AuNR heating quantitatively agrees with the theoretical calculations. Furthermore, the distance at which the field decays from the surface of the smallest AuNR is very short, suggesting that effective experimental heating of the solution, when exposed to NIR radiation, will be low for this small particle.

Testing our theoretical results, we determined the efficacy of the different sized AuNRs as photothermal contrast agents, using an *in vitro* malignant cell model. The 28 × 8 nm AuNRs showed the greatest efficacy, exhibiting greater cell death upon NIR laser irradiation compared to the more conventional AuNRs (38 × 11 nm) or the smallest AuNRs (17 × 5 nm). These results, in agreement with theoretical and photothermal heating experiments using the different rods, suggest that the median size AuNR (28 × 8 nm) is the most ideal for plasmonic photothermal therapy.

EXPERIMENTAL METHODS

Gold Nanorod (AuNR) Synthesis and PEG Conjugation. The large AuNRs were synthesized via the seed-mediated growth method.[44] Briefly, a seed solution consisting of 7.5 mL of 0.2 M CTAB, 2.5 mL of 1.0 mM $HAuCl_4$, and 600 μL of 0.01 M $NaBH_4$ is prepared, followed by a growth solution containing 100 mL of 1.0 mM $HAuCl_4$, 100 mL of 0.2 M CTAB, 5 mL of 4.0 mM silver nitrate, and 1.4 mL of 78.8 mM ascorbic acid. A 240 μL volume of the seed solution is added to the growth solution, producing AuNRs approximately 38 nm in length and 11 nm in width, as displayed in Figure 1A. The surface plasmon resonance (SPR) of these AuNRs is around 740 nm.

Two different, smaller, AuNRs were synthesized by a seedless growth method.[36] In this method, the growth solution was kept at an acidic pH and sodium borohydride was added instead of a seed solution, for simultaneous seed formation and AuNR growth. To obtain AuNRs approximately 28 nm in length and 8 nm in width (Figure 1B), 300 μL of 0.01 M $NaBH_4$ was prepared and added to an acidic growth solution containing 160 μL of 37% HCl, 100 mL of 1.0 mM $HAuCl_4$, 100 mL of 0.2 M CTAB, 5 mL of 4.0 mM silver nitrate, and 1.4 mL of 78.8 mM ascorbic acid. The SPR of these AuNRs is around 770 nm. To obtain AuNRs approximately 17 nm in length and 5 nm in width (Figure 1C), 150 μL of 0.01 M $NaBH_4$ was prepared and added to an acidic growth solution containing 160 μL of 37% HCl, 50 mL of 1.0 mM $HAuCl_4$, 100 mL of 0.2 M CTAB, 5 mL of 4.0 mM silver nitrate, and 700 μL of 78.8 mM ascorbic acid. The SPR of these AuNRs is around 755 nm. All CTAB-stabilized AuNRs were also purified by centrifugation and redispersed in dI H_2O.

After purification, the various AuNRs were functionalized with polyethylene glycol (mPEG-SH, MW 5000, Laysan Bio, Inc.) and left on a shaker overnight, after which they were centrifuged and redispersed in dI H_2O.

Photothermal Heating of AuNRs in Solution. The as-synthesized (i.e., CTAB capped) AuNRs were diluted in dI H_2O, such that the three AuNR solutions had either the same concentration of particles or the same optical density (OD). The AuNR concentrations were calculated on the basis of the previously determined extinction coefficients for the 17 × 5 nm AuNRs (7.9×10^7 M^{-1} cm^{-1}), 28 × 8 nm AuNRs[36] (1.5×10^8 M^{-1} cm^{-1}), and 38 × 11 nm AuNRs[45] (4.0×10^9 M^{-1} cm^{-1}). A 500 μL volume of AuNRs, in a microcentrifuge tube, was exposed to a near-infrared (NIR) cw laser (808 nm) at 5.8 W/cm^2 (spot size around 5.6 mm) at increasing irradiation times. The temperature increase of the solution was measured by placing a 33 gauge hypodermic thermocouple (Omega) directly

dx.doi.org/10.1021/jp409298f | J. Phys. Chem. B 2014, 118, 1319−1326

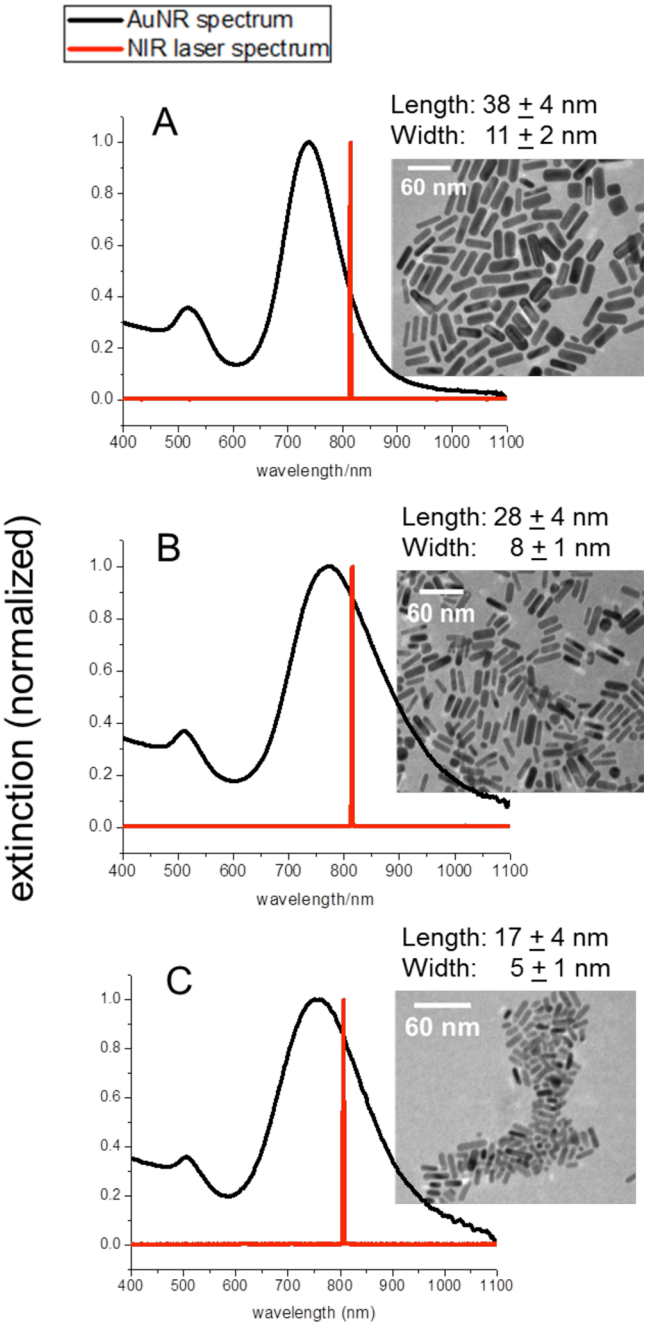

Figure 1. UV−vis spectra of AuNRs (black) as well as the NIR cw laser spectrum (red) (with corresponding TEM images, scale bar: 60 nm). (A) 38 × 11 nm AuNRs with longitudinal plasmon resonance at 740 nm. (B) 28 × 8 nm AuNRs with longitudinal plasmon resonance at 770 nm. (C) 17 × 5 nm AuNRs with longitudinal plasmon resonance at 755 nm.

into the AuNR solution. A 500 μL solution of dI H_2O was also measured, and the temperature increase of the H_2O was subtracted from that of the AuNR solutions in order to account for any heat generated from the laser itself. For normalization purposes, all initial temperatures were 24 ± 1 °C. TEM images and UV−vis spectra indicate that photothermal heating did not alter the structure or spectra of the AuNRs (data not shown).

AuNR Heating in Cell Culture and Cell Viability Assay. Human oral squamous cell carcinoma (HSC-3) cells were maintained in Dulbecco's modified Eagle's medium (DMEM, Mediatech) supplemented with 10% v/v fetal bovine serum (FBS, Mediatech) and 1% v/v antimycotic solution (Mediatech). The cell culture was kept in a 37 °C, 5% CO_2, humidified incubator. HSC-3 cells were grown in 96-well tissue culture plates overnight. After which, the growth media was removed and replaced with growth media containing PEG-AuNRs at optical densities of 0.5 (17 × 5, 28 × 8, and 38 × 11 nm AuNRs) and 1.5 (38 × 11 nm AuNRs). The UV−vis spectra of PEG-AuNRs in growth media were not significantly altered by changing their environment from water to growth media (see the Supporting Information, Figure S2), confirming their stability. After a 2 h incubation time, the cells were exposed to a NIR cw laser (808 nm) at 5.8 W/cm^2 (spot size around 5.6 mm) at increasing irradiation times. The temperature increase was measured by placing a 33 gauge hypodermic thermocouple (Omega) directly into the culture medium. For normalization purposes, all initial temperatures were 32 ± 1 °C. The cell viability was determined via an XTT cell viability assay kit (Biotium, Inc.), according to the manufacturer's protocol.

Statistical Analysis. Results are expressed as the mean ± standard deviations of three independent experiments. Statistical significance (i.e., *p*-value) was calculated by a *t-test calculator* (GraphPad Software, Inc.). Statistically significant data is indicated by * (*p*-value <0.05).

THEORETICAL METHODS

DDA Calculations. The optical response of a gold nanorod with varying dimensions (38 × 10 nm, 25 × 7 nm, and 18 × 4 nm) was calculated using the DDA method with the DDSCAT 6.1 code offered publicly by Draine and Flatau[41] with modifications by Goodman[42] and Schatz.[43] The dielectric values for gold reported by Johnson and Christy[46] were used. The incident light is always polarized along the length of the particle (i.e., longitudinal mode) in this report, and the medium surrounding the particle was represented as water with a refractive index of 1.333. The nanorods were modeled as cylinders with hemispherical end-caps.

RESULTS AND DISCUSSION

Size-Dependent Photothermal Heat Conversion: Experiment. Gold nanorods (AuNRs) were synthesized with lengths of around 38 nm (Figure 1A), 28 nm (Figure 1B), and 17 nm (Figure 1C). The longitudinal plasmon resonances of the different AuNRs are around 740, 770, and 755 nm, respectively. With the knowledge that the percentage of the extinction that a plasmonic nanoparticle can convert into heat increases as nanoparticle size is decreased,[30,31] we expected that the smaller AuNRs would generate more heat than the larger AuNRs when exposed to near-infrared (NIR) cw laser irradiation (808 nm). However, we also know that the value of the extinction itself decreases as the nanoparticle size decreases; thus, it is expected that there is an optimum AuNR size that is most efficient at generating heat via NIR irradiation. Therefore, we determined the photothermal heat conversion factor, per particle, in order to directly compare the difference in heat generated by the different AuNRs upon NIR irradiation at increasing time intervals. This was done by preparing 10 nM solutions of the three different AuNRs (see the Experimental Methods for details). The solutions were then exposed to NIR radiation at 5.8 W/cm^2 (spot size around 5.6 mm). Upon determining the increase in temperature for the AuNR solutions, the change in temperature per AuNR was calculated and multiplied by a factor of 10^{11} in order to simplify the values

dx.doi.org/10.1021/jp409298f | J. Phys. Chem. B 2014, 118, 1319−1326

being compared. Figure 2 compares the photothermal heat conversion factor of each different AuNR tested in this work.

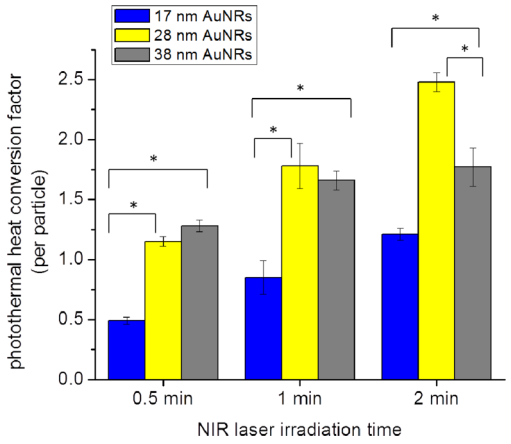

Figure 2. Photothermal heat conversion factor determined (per particle) for the 17 × 5 nm AuNRs (17 nm, blue), 28 × 8 nm AuNRs (28 nm, yellow), and 38 × 11 nm AuNRs (38 nm, gray) at increasing NIR laser irradiation time. All initial temperatures were 24 ± 1 °C. Statistical significance ($p < 0.05$) indicated by *.

As the NIR laser irradiation time is increased, the photothermal heat conversion factor increases, especially for AuNRs that are 28 nm in length. At an exposure time of 2 min, the photothermal heat conversion factor for the 17, 28, and 38 nm AuNRs is 1.21, 2.48, and 1.77, respectively. This indicates that the 28 nm AuNRs exhibit the greatest photothermal heat conversion, which was unexpected, since we expected that the smaller AuNRs would generate more heat upon NIR laser irradiation. Therefore, a thorough investigation of the plasmonic properties of these three different nanoparticles, as well as their efficacy in plasmonic photothermal therapy, is warranted.

Size-Dependent Electromagnetic Field: Theory. Since the experimental photothermal heat conversion factor per particle could potentially correspond to the field enhancement around the particle, the discrete dipole approximation (DDA) was used to generate field contour plots for three different AuNRs (38 × 10 nm, 25 × 7 nm, and 18 × 4 nm) shown in Figure 3. The laser wavelength (808 nm) used for experimental heating did not exactly correspond to the plasmon resonances of the AuNRs; therefore, in the DDA calculations, the AuNRs were similarly excited off resonance. We also compared the field enhancement values for the three AuNRs (38 × 10, 25 × 7, and 18 × 4 nm) on resonance, at their respective resonance wavelengths (786, 757, and 865 nm), which can be seen in Figure S1 of the Supporting Information. Experimentally, the particles were excited at 808 nm (i.e., off resonance), at which point the extinction value of the AuNRs was decreased by 15% (18 × 4 nm), 6% (25 × 7 nm), and 46% (38 × 10 nm), compared to their maximum value (Figure 1). In order to account for this theoretically, we calculated the electromagnetic field contours at 804 nm for the 38 × 10 nm AuNR, 761 nm for the 25 × 7 nm AuNR, and 875 nm for the 18 × 4 nm AuNR, which are the wavelengths where the DDA calculated extinction decreased by 46, 6, and 15% from its maximum value, respectively. As shown in Figure 3, the maximum fields generated are 3500, 5220, and 5480 for the 38 × 10, 25 × 7, and 18 × 4 nm AuNRs, respectively. It should also be noted that the field maximum for the 25 × 7 nm AuNRs is 1.5 times

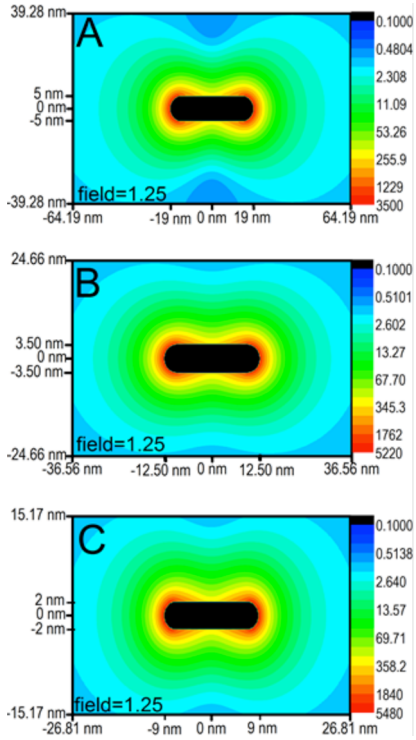

Figure 3. Field contour plots for the longitudinal mode of the different AuNRs, with particle dimensions indicated and the field decaying to 1.25 at the extremities of each plot. (A) The field maximum of the 38 × 10 nm AuNR (calculated at 804 nm) is 3500. (B) The field maximum of the 25 × 7 nm AuNR (calculated at 761 nm) is 5220. (C) The field maximum of the 18 × 4 nm AuNR (calculated at 875 nm) is 5480.

that of the 38 × 10 nm AuNRs, which is consistent with the experimentally determined photothermal heat conversion factor being 1.4 times greater than that of the 38 nm AuNRs.

This trend of increasing electromagnetic field with decreasing particle size is expected but does not necessarily correlate with what was seen experimentally for the photothermal heat conversion factor (Figure 2). The smallest AuNRs had the smallest photothermal heat conversion factor, suggesting that they would have the weakest electromagnetic field, but they in fact have the strongest field according to our calculations. Therefore, another factor involved in the photothermal heat conversion could be the distance at which the field decays. In order to achieve overall heating of the surrounding medium, as opposed to local heating around the particle, the field needs to extend a certain distance away from the particle surface, such that field coupling between particles can occur, resulting in effective solution heating. Because the field decays exponentially from the particle surface, both the maximum field enhancement value and particle size play a role in how far the enhanced field extends away from the particle. Therefore, also shown in Figure 3 are the distances at which the field has decayed to a value of 1.25. The smallest AuNR (18 × 4 nm) does indeed have the strongest field, but it only extends 15.17 nm from the nanoparticle surface before it has decayed to a value of 1.25, while the 25 × 7 nm AuNR has a slightly weaker field maximum, but the field extends out to 24.66 nm from the nanoparticle surface. The largest AuNR (38 × 10 nm) has the weakest field maximum but has the largest distance at which the field decays to 1.25 (39.28 nm).

dx.doi.org/10.1021/jp409298f | J. Phys. Chem. B 2014, 118, 1319−1326

The distance at which the field decays is relevant in terms of the experimental photothermal heat conversion determined for these AuNRs, such that, although the smallest AuNR (18 × 4 nm) has the strongest field, it does not extend far enough from the nanoparticle surface to achieve sufficient overall experimental heating of the 10 nM AuNR solution. The concentration of the smallest AuNRs must be at least 20 nM (i.e., an increase in the particle aggregation) in order for the solution temperature to reach that which is comparable to the other AuNRs at 10 nM concentrations (see the Supporting Information, Table S1). The necessity for this prohibitively high concentration of the smallest AuNRs renders these particles impractical for applications in which overall heating of a solution is desired. These results suggest the importance of aggregation for effective heating of plasmonic nanoparticles in solution. Although the field intensity at the surface is highest for the smallest AuNR, the short distance at which this field extends from the surface prevents field coupling between AuNRs in solution, thus reducing effective overall heating.

Size-Dependent Absorbance: Theory. To further investigate the plasmonic properties of the different sized AuNRs, which influence their differences in photothermal heat conversion, DDA calculations were done to determine the contributions of absorbance and scattering to the total extinction of the particles. In Figure 4, the DDA spectra show that the plasmon resonances for the longitudinal mode of the 38, 25, and 18 nm AuNRs are at 786, 757, and 865 nm, respectively. Additionally, the total extinction increases with increasing particle size, with the contribution from scattering also increasing with particle size, as expected.[30,31] The absorbance:scattering ratio for the 38, 25, and 18 nm AuNRs is 63.8, 204, and 921, respectively. Therefore, comparing the smaller AuNRs to the 38 nm AuNRs, the absorbance:scattering ratio is 3.2 times greater for the 25 nm AuNRs and 14.4 times greater for the 18 nm AuNRs. This suggests that the experimental photothermal heating of AuNR solutions would be equivalent when the optical density of 38 nm AuNRs is about 3 times that of the 28 nm AuNRs and about 14 times that of the 17 nm AuNRs.

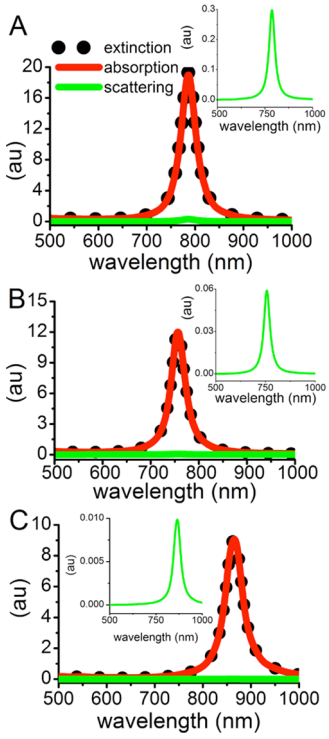

Figure 4. DDA extinction (black dots), absorption (red line), and scattering (green line, and shown in inset) spectra for the longitudinal mode of the different AuNRs in water. (A) The 38 × 10 nm AuNR has an absorbance:scattering ratio of 63.8. (B) The 25 × 7 nm AuNR has an absorbance:scattering ratio of 204. (C) The 18 × 4 nm AuNR has an absorbance:scattering ratio of 921.

Size-Dependent Absorbance: Experiment. In order to experimentally correlate the calculated absorbance:scattering ratio to photothermal heat conversion, we looked at the NIR photothermal heating of the different sized AuNRs at varying extinctions (optical densities). Specifically, as shown in Figure 5, the smaller AuNRs (17 and 28 nm) with an OD of 0.5

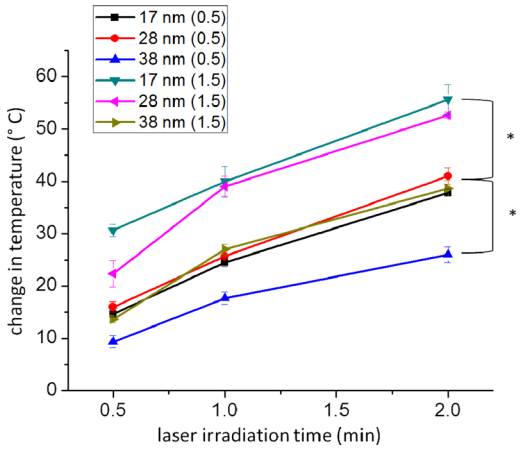

Figure 5. Temperature change induced by plasmonic photothermal heating of different AuNRs (17, 28, and 38 nm in length) at different optical densities (0.5 and 1.5) and increasing NIR laser irradiation times. All initial temperatures were 24 ± 1 °C. Statistical significance between different sized AuNRs and optical densities at 2 min of laser irradiation ($p < 0.5$) is indicated by *.

demonstrate statistically significant enhanced photothermal heating (increase by 15 °C) compared to that of the 38 nm AuNRs at OD 0.5 after 2 min of NIR laser exposure. Interestingly, the small AuNRs (17 and 28 nm) at OD 0.5 and the large AuNRs (38 nm) with OD 1.5 exhibit about the same change in temperature after 2 min of NIR laser exposure. This shows that a 3-fold increase in the optical density, the same difference in the absorbance:scattering ratio predicted by DDA, was needed to achieve the same temperature increase. Again, the 28 × 8 and 38 × 11 nm AuNRs experimentally agree with the theoretical calculations for the 25 × 7 and 38 × 10 nm AuNRs. On the basis of the absorbance:scattering ratios calculated for individual particles, the 17 × 4 nm AuNRs would exhibit a higher temperature increase than the other larger AuNRs, but this is not observed. Again, the aggregation of plasmonic particles in solution is suggested as an important factor governing effective heat conversion, such that the distance at which the field extends from the surface of the AuNR needs to be far enough to allow for coupling with fields of nearby AuNRs, which we show is not the case for this small size AuNR.

Size-Dependent *In Vitro* Plasmonic Photothermal Efficacy in HSC-3 Cancer Cells. The enhanced photothermal heat conversion observed with the 28 nm AuNRs suggests that

dx.doi.org/10.1021/jp409298f | J. Phys. Chem. B 2014, 118, 1319−1326

these nanoparticles would have great potential as photothermal contrast agents in plasmonic photothermal therapy (PPTT). Therefore, we used HSC-3 cells (oral squamous cell carcinoma), *in vitro*, to compare the efficacy of the three different PEG-AuNRs for photothermal ablation. Our *in vitro* experiments essentially represent a situation in which the malignant cells are surrounded by a solution containing the photothermal contrast agents (i.e., PEG-AuNRs). These *in vitro* results can perhaps be expanded to the *in vivo* regime, in which a tumor is directly injected with AuNRs. HSC-3 cells were treated with the three different PEG-AuNRs for 2 h before exposure to NIR radiation. The cells were irradiated at 5.8 W/cm^2 for 0.5, 1, and 2 min, and the temperature increase was directly measured in the cell culture using a hypodermic thermocouple. The change in temperature observed for the different PEG-AuNRs in the cell culture is shown in Figure 6.

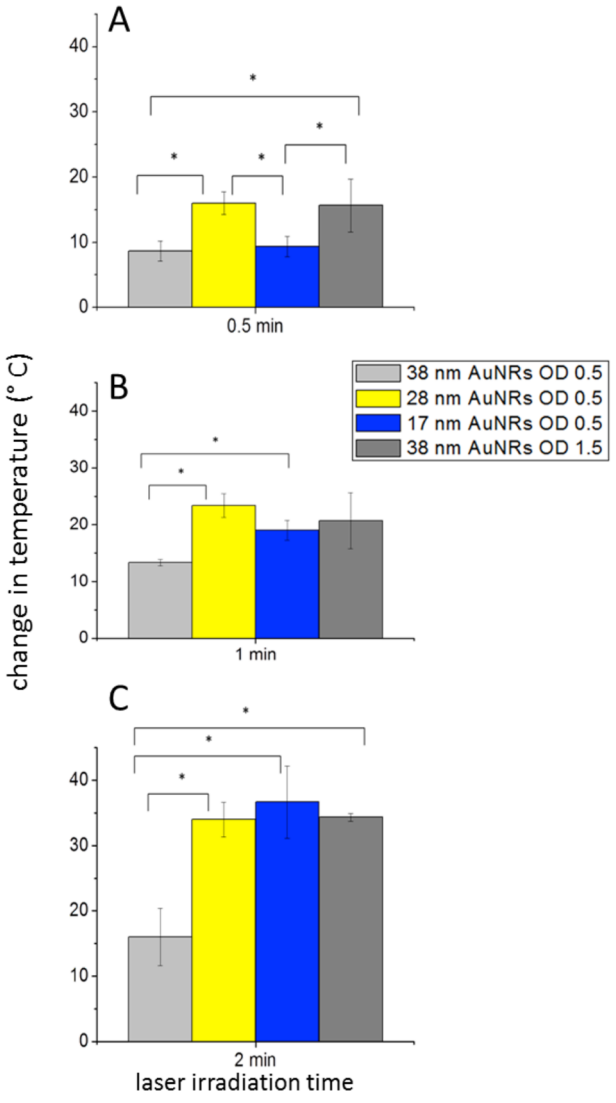

Figure 6. Temperature change of the cell culture medium containing different AuNRs. AuNRs 38 nm in length at OD 0.5 (light gray), AuNRs 28 nm in length at OD 0.5 (yellow), AuNRs 17 nm in length at OD 0.5 (blue), and AuNRs 38 nm in length at OD 1.5 (dark gray) were all exposed to NIR laser irradiation at increasing lengths of time. All initial temperatures were 32 ± 1 °C. Statistical significance between different sized AuNRs and optical densities ($p < 0.5$) is indicated by * above bars.

It is clear that, at the same OD, the temperature increase is greater for the smaller PEG-AuNRs (17 and 28 nm) than for the large PEG-AuNRs (38 nm). When the optical density of the large PEG-AuNRs was made to be 3 times that of the smaller PEG-AuNRs, as suggested by the absorbance:scattering ratios determined with DDA (Figure 4) and the photothermal heating in solution (Figure 5), the temperature increase was similar to that of both smaller PEG-AuNRs. These temperature increases indicate hyperthermia, which is a well-established mode of tumor tissue ablation.[10−12] Therefore, it is important to assess the outcome of these temperature increases by determining the cell death associated with the AuNR-induced plasmonic photothermal hyperthermia. As shown in Figure 7, the cell viability decreases with increasing NIR laser irradiation times, as would be expected. Also interesting here is that the greatest amount of cell death, at any exposure time, is observed for the 28 nm PEG-AuNRs with an OD of 0.5. The 17 nm PEG-AuNRs with an optical density of 0.5 and the 38 nm PEG-AuNRs with an optical density of 1.5 show a higher cell viability but not statistically significant enough to claim it as different from that of the 28 nm PEG-AuNRs (OD 0.5). The 38 nm PEG-AuNRs at OD 0.5 do not show any significant change in cell viability upon NIR laser exposure at any of the exposure times tested here.

CONCLUSION

We have clearly shown, both theoretically and experimentally *in vitro*, that there are limitations in the AuNR size when choosing the best photothermal contrast agent for use in plasmonic photothermal therapy (PPTT). It is clear from the agreement between experimental and theoretical results presented above that the 28 nm AuNRs are capable of producing more heat via NIR cw laser irradiation than the larger, more conventional (38 nm) AuNRs and even the smaller (17 nm) AuNRs. The initial disagreement between theory and experiment for the smallest individual AuNR investigated (17 nm) suggests the importance of nanoparticle aggregation in solution. Although the AuNR with dimensions of 17 × 5 nm has a high absorbance:scattering ratio and an extremely intense electromagnetic field at its surface, this field does not extend far enough from the surface to allow for coupling between fields of adjacent particles (i.e., aggregated particles) in solution, for effective photothermal heat conversion to occur. With AuNRs having dimensions around 38 × 11 nm, the particle is so large that, although it exhibits a high extinction cross section, most of the extinction is attributed to scattering instead of absorption, and thus less heat is generated upon experimental NIR laser irradiation. The AuNR having dimensions of around 28 × 8 nm exhibits the most ideal size for the application as a photothermal contrast agent. This size nanorod has an intense electromagnetic field that extends far enough from the particle surface to allow for field coupling between particle aggregates, resulting in enhanced experimental photothermal heating in solution. In addition, with this size nanorod, although having a lower extinction cross section, the majority of the extinction is attributed to absorption, allowing for high photothermal heat conversion upon experimental NIR laser irradiation. These theoretical and experimental observations lead to the conclusion, as shown in our *in vitro* experiments, that the 28 × 8 nm AuNRs are more effective photothermal contrast agents than either the 38 × 11 or 17 × 5 nm AuNRs, for the photothermal ablation of cancer cells. A full assessment of these newly investigated AuNRs should be done in order to

dx.doi.org/10.1021/jp409298f | J. Phys. Chem. B 2014, 118, 1319−1326

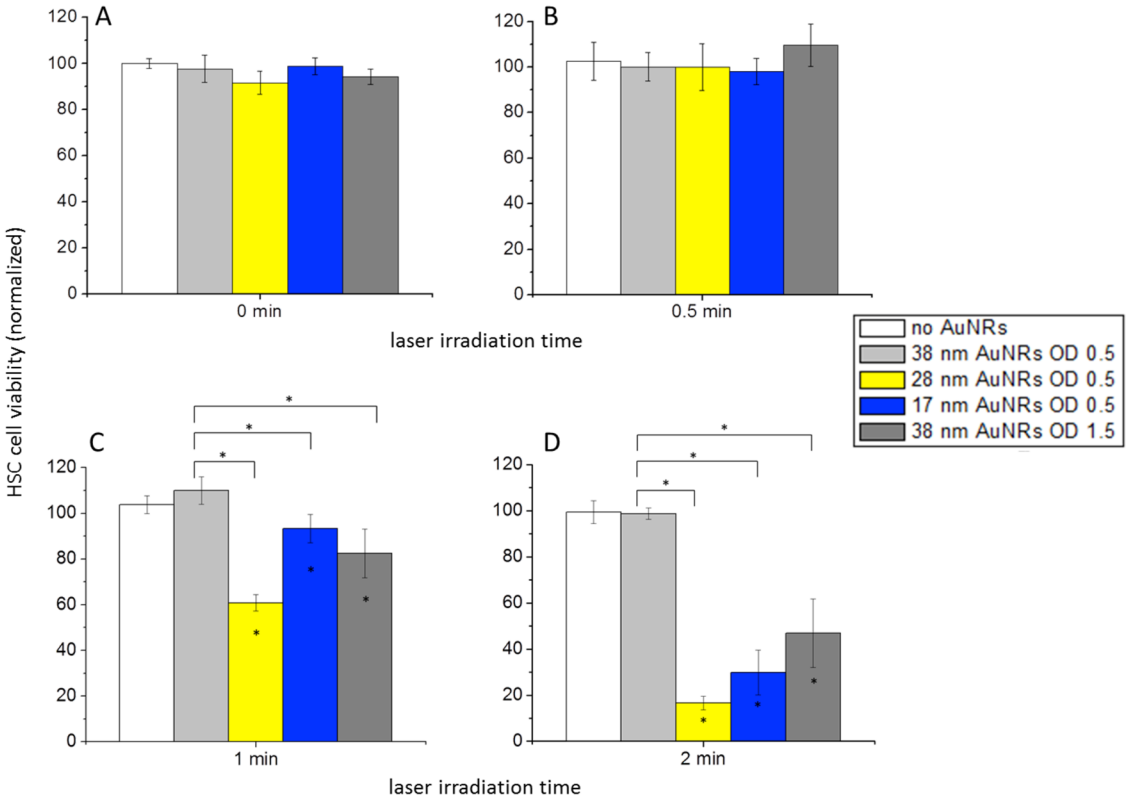

Figure 7. Cell viability determined for HSC cells treated with different AuNRs and subjected to PPTT via NIR laser irradiation. Cells treated with AuNRs 38 nm in length at OD 0.5 shown in light gray, AuNRs 28 nm in length at OD 0.5 shown in yellow, AuNRs 17 nm in length at OD 0.5 shown in blue, and AuNRs 38 nm in length at OD 1.5 shown in dark gray. Statistical significance ($p < 0.05$) indicated by *. Statistical significance with respect to control (no AuNRs) indicated inside bars. Statistical significance between different treatments indicated above bars.

determine their efficacy *in vivo* as well as their toxicity, compared with the more conventional photothermal contrast agents. This work has the potential to aid in the development of a more effective PPTT for the treatment of disease.

■ ASSOCIATED CONTENT

Supporting Information

A table of additional temperature measurements as well as additional theoretical results and gold nanorod UV−vis spectra. This material is available free of charge via the Internet at http://pubs.acs.org.

■ AUTHOR INFORMATION

Corresponding Author

*Address: 901 Atlantic Drive, Atlanta, GA, 30332-0400. Phone: 404-894-0292. Fax: 404-894-7452. E-mail: melsayed@gatech.edu.

Author Contributions

†These authors contributed equally.

Notes

The authors declare no competing financial interest.

■ ACKNOWLEDGMENTS

The authors would like to thank the National Institutes of Health National Cancer Institute under Grant No. CNPP U01CA151802, the AFOSR Center of Excellence on BIONIC under Grant No. FA9550-09-1-0162, and AFRL/RX for supporting this research.

■ REFERENCES

(1) Huang, X. H.; Jain, P. K.; El-Sayed, I. H.; El-Sayed, M. A. Plasmonic Photothermal Therapy (PPTT) Using Gold Nanoparticles. *Lasers Med. Sci.* **2008**, *23*, 217−228.

(2) El-Sayed, M. A. Some Interesting Properties of Metals Confined in Time and Nanometer Space of Different Shapes. *Acc. Chem. Res.* **2001**, *34*, 257−264.

(3) Link, S.; El-Sayed, M. A. Shape and Size Dependence of Radiative, Non-Radiative and Photothermal Properties of Gold Nanocrystals. *Int. Rev. Phys. Chem.* **2000**, *19*, 409−453.

(4) Connor, E. E.; Mwamuka, J.; Gole, A.; Murphy, C. J.; Wyatt, M. D. Gold Nanoparticles are Taken Up by Human Cells But Do Not Cause Acute Cytotoxicity. *Small* **2005**, *1*, 325−327.

(5) Khan, J. A.; Pillai, B.; Das, T. K.; Singh, Y.; Maiti, S. Molecular Effects of Uptake of Gold Nanoparticles in HeLa Cells. *ChemBioChem* **2007**, *8*, 1237−1240.

(6) Shukla, R.; Bansal, V.; Chaudhary, M.; Basu, A.; Bhonde, R. R.; Sastry, M. Biocompatibility of Gold Nanoparticles and Their Endocytotic Fate Inside the Cellular Compartment: A Microscopic Overview. *Langmuir* **2005**, *21*, 10644−10654.

(7) Jain, P. K.; Huang, X. H.; El-Sayed, I. H.; El-Sayed, M. A. Noble Metals on the Nanoscale: Optical and Photothermal Properties and Some Applications in Imaging, Sensing, Biology, and Medicine. *Acc. Chem. Res.* **2008**, *41*, 1578−1586.

(8) Hartland, G. V. Optical Studies of Dynamics in Noble Metal Nanostructures. *Chem. Rev.* **2011**, *111*, 3858−3887.

(9) El-Sayed, I. H.; Huang, X. H.; El-Sayed, M. A. Selective Laser Photo-Thermal Therapy of Epithelial Carcinoma Using Anti-EGFR Antibody Conjugated Gold Nanoparticles. *Cancer Lett.* **2006**, *239*, 129−135.

(10) Nolsoe, C. P.; Torp-Pedersen, S.; Burcharth, F.; Horn, T.; Pedersen, S.; Christensen, N. E.; Olldag, E. S.; Andersen, P. H.; Karstrup, S.; Lorentzen, T.; et al. Interstitial Hyperthermia of

Colorectal Liver Metastases with a US-Guided Nd-YAG Laser with a Diffuser Tip: A Pilot Clinical Study. *Radiology* **1993**, *187*, 333−337.
(11) O'Neal, D. P.; Hirsch, L. R.; Halas, N. J.; Payne, J. D.; West, J. L. Photo-Thermal Tumor Ablation in Mice Using Near Infrared-Absorbing Nanoparticles. *Cancer Lett.* **2004**, *209*, 171−176.
(12) Dickerson, E. B.; Dreaden, E. C.; Huang, X. H.; El-Sayed, I. H.; Chu, H. H.; Pushpanketh, S.; McDonald, J. F.; El-Sayed, M. A. Gold Nanorod Assisted Near-Infrared Plasmonic Photothermal Therapy (PPTT) of Squamous Cell Carcinoma in Mice. *Cancer Lett.* **2008**, *269*, 57−66.
(13) Gobin, A. M.; Lee, M. H.; Halas, N. J.; James, W. D.; Drezek, R. A.; West, J. L. Near-Infrared Resonant Nanoshells for Combined Optical Imaging and Photothermal Cancer Therapy. *Nano Lett.* **2007**, *7*, 1929−1934.
(14) Dreaden, E. C.; Alkilany, A. M.; Huang, X. H.; Murphy, C. J.; El-Sayed, M. A. The Golden Age: Gold Nanoparticles for Biomedicine. *Chem. Soc. Rev.* **2012**, *41*, 2740−2779.
(15) Dreaden, E. C.; Mackey, M. A.; Huang, X. H.; Kang, B.; El-Sayed, M. A. Beating Cancer in Multiple Ways Using Nanogold. *Chem. Soc. Rev.* **2011**, *40*, 3391−3404.
(16) Chen, J. Y.; Glaus, C.; Laforest, R.; Zhang, Q.; Yang, M. X.; Gidding, M.; Welch, M. J.; Xia, Y. Gold Nanocages as Photothermal Transducers for Cancer Treatment. *Small* **2010**, *6*, 811−817.
(17) von Maltzahn, G.; Park, J. H.; Agrawal, A.; Bandaru, N. K.; Das, S. K.; Sailor, M. J.; Bhatia, S. N. Computationally Guided Photothermal Tumor Therapy Using Long-Circulating Gold Nanorod Antennas. *Cancer Res.* **2009**, *69*, 3892−3900.
(18) Hirsch, L. R.; Stafford, R. J.; Bankson, J. A.; Sershen, S. R.; Rivera, B.; Price, R. E.; Hazle, J. D.; Halas, N. J.; West, J. L. Nanoshell-Mediated Near-Infrared Thermal Therapy of Tumors Under Magnetic Resonance Guidance. *Proc. Natl. Acad. Sci. U.S.A.* **2003**, *100*, 13549−13554.
(19) Lu, W.; Xiong, C.; Zhang, G.; Huang, Q.; Zhang, R.; Zhang, J. Z.; Li, C. Targeted Photothermal Ablation of Murine Melanomas with Melanocyte-Stimulating Hormone Analog-Conjugated Hollow Gold Nanospheres. *Clin. Cancer Res.* **2009**, *15*, 876−886.
(20) Pitsillides, C. M.; Joe, E. K.; Wei, X. B.; Anderson, R. R.; Lin, C. P. Selective Cell Targeting with Light-Absorbing Microparticles and Nanoparticles. *Biophys. J.* **2003**, *84*, 4023−4032.
(21) Weissleder, R. A Clearer Vision for In Vivo Imaging. *Nat. Biotechnol.* **2001**, *19*, 316−317.
(22) Burda, C.; Chen, X. B.; Narayanan, R.; El-Sayed, M. A. Chemistry and Properties of Nanocrystals of Different Shapes. *Chem. Rev.* **2005**, *105*, 1025−1102.
(23) Loo, C.; Lowery, A.; Halas, N. J.; West, J.; Drezek, R. Immunotargeted Nanoshells for Integrated Cancer Imaging and Therapy. *Nano Lett.* **2005**, *5*, 709−711.
(24) Chen, J. Y.; Wang, D. L.; Xi, J. F.; Au, L.; Siekkinen, A.; Warsen, A.; Li, Z. Y.; Zhang, H.; Xia, Y. N.; Li, X. D. Immuno Gold Nanocages with Tailored Optical Properties for Targeted Photothermal Destruction of Cancer Cells. *Nano Lett.* **2007**, *7*, 1318−1322.
(25) Murphy, C. J.; San, T. K.; Gole, A. M.; Orendorff, C. J.; Gao, J. X.; Gou, L.; Hunyadi, S. E.; Li, T. Anisotropic Metal Nanoparticles: Synthesis, Assembly, and Optical Applications. *J. Phys. Chem. B* **2005**, *109*, 13857−13870.
(26) Nikoobakht, B.; El-Sayed, M. A. Preparation and Growth Mechanism of Gold Nanorods (NRs) Using Seed-Mediated Growth Method. *Chem. Mater.* **2003**, *15*, 1957−1962.
(27) Wiley, B.; Sun, Y. G.; Xia, Y. N. Synthesis of Silver Nanostructures with Controlled Shapes and Properties. *Acc. Chem. Res.* **2007**, *40*, 1067−1076.
(28) Huang, X. H.; El-Sayed, I. H.; Qian, W.; El-Sayed, M. A. Cancer Cell Imaging and Photothermal Therapy in the Near-Infrared Region by Using Gold Nanorods. *J. Am. Chem. Soc.* **2006**, *128*, 2115−2120.
(29) Chen, J.; Wang, D.; Xi, J.; Au, L.; Siekkinen, A.; Warsen, A.; Li, Z. Y.; Zhang, H.; Xia, Y.; Li, X. Immuno Gold Nanocages with Tailored Optical Properties for Targeted Photothermal Destruction of Cancer Cells. *Nano Lett.* **2007**, *7*, 1318−1322.
(30) Jain, P. K.; Lee, K. S.; El-Sayed, I. H.; El-Sayed, M. A. Calculated Absorption and Scattering Properties of Gold Nanoparticles of Different Size, Shape, and Composition: Applications in Biological Imaging and Biomedicine. *J. Phys. Chem. B* **2006**, *110*, 7238−7248.
(31) Lee, K. S.; El-Sayed, M. A. Dependence of the Enhanced Optical Scattering Efficiency Relative to that of Absorption for Gold Metal Nanorods on Aspect Ratio, Size, End-Cap Shape, and Medium Refractive Index. *J. Phys. Chem. B* **2005**, *109*, 20331−20338.
(32) Hu, M.; Chen, J.; Li, Z. Y.; Au, L.; Hartland, G. V.; Li, X.; Marquez, M.; Xia, Y. Gold Nanostructures: Engineering Their Plasmonic Properties for Biomedical Applications. *Chem. Soc. Rev.* **2006**, *35*, 1084−1094.
(33) Hao, E.; Schatz, G. C. Electromagnetic Fields Around Silver Nanoparticles and Dimers. *J. Chem. Phys.* **2004**, *120*, 357−366.
(34) Kelly, K. L.; Coronado, E.; Zhao, L. L.; Schatz, G. C. The Optical Properties of Metal Nanoparticles: The Influence of Size, Shape, and Dielectric Environment. *J. Phys. Chem. B* **2003**, *107*, 668−677.
(35) Near, R.; Hayden, S.; El-Sayed, M. A. Extinction vs Absorption: Which is the Indicator of Plasmonic Field Strength for Silver Nanocubes? *J. Phys. Chem. C* **2012**, *116*, 23019−23026.
(36) Ali, M. R. K.; Snyder, B.; El-Sayed, M. A. Synthesis and Optical Properties of Small Au Nanorods Using a Seedless Growth Technique. *Langmuir* **2012**, *28*, 9807−9815.
(37) Halas, N. J. Playing With Plasmons. Tuning the Optical Resonant Properties of Metallic Nanoshells. *MRS Bull.* **2005**, *30*, 362−367.
(38) Olson, T. Y.; Schwartzberg, A. M.; Orme, C. A.; Talley, C. E.; O'Connell, B.; Zhang, J. Z. Hollow Gold-Silver Double-Shell Nanospheres: Structure, Optical Absorption, and Surface-Enhanced Raman Scattering. *J. Phys. Chem. C* **2008**, *112*, 6319−6329.
(39) Sun, Y. G.; Mayers, B.; Xia, Y. N. Metal Nanostructures with Hollow Interiors. *Adv. Mater.* **2003**, *15*, 641−646.
(40) Wan, D. H.; Chen, H. L.; Lin, Y. S.; Chuang, S. Y.; Shieh, J.; Chen, S. H. Using Spectroscopic Ellipsometry to Characterize and Apply the Optical Constants of Hollow Gold Nanoparticles. *ACS Nano* **2009**, *3*, 960−970.
(41) Draine, B. T.; Flatau, P. J. Discrete-Dipole Approximation for Scattering Calculations. *J. Opt. Soc. Am. A* **1994**, *11*, 1491−1499.
(42) Goodman, J. J.; Draine, B. T.; Flatau, P. J. Application of Fast-Fourier-Transform Techniques to the Discrete-Dipole Approximation. *Opt. Lett.* **1991**, *16*, 1198−1200.
(43) Shuford, K. L., Ratner, M. A., and Schatz, G. C. Multipolar Excitation in Triangular Nanoprisms. *J. Chem. Phys.* **2005**, *123*.
(44) Huang, X. H.; Neretina, S.; El-Sayed, M. A. Gold Nanorods: From Synthesis and Properties to Biological and Biomedical Applications. *Adv. Mater.* **2009**, *21*, 4880−4910.
(45) Orendorff, C. J.; Murphy, C. J. Quantitation of Metal Content in the Silver-Assisted Growth of Gold Nanorods. *J. Phys. Chem. B* **2006**, *110*, 3990−3994.
(46) Johnson, P. B.; Christy, R. W. Optical Constants of Noble Metals. *Phys. Rev. B* **1972**, *6*, 4370−4379.